Winter Euro-Atlantic blocking activity less sensitive to climate change than previously evaluated

Simon L. L. Michel*[1], Anna S. von der Heydt[1], Henk A. Dijkstra[1]

1: Institute for Marine and Atmospheric Research Utrecht - Utrecht University

*s.l.l.michel@uu.nl

Abstract:

Winter Euro-Atlantic atmospheric blocking events have significant socioeconomical impacts as they cause various types of weather extremes in a range of regions. According to current climate projections, fewer of these blocking events will occur as temperatures rise. However, the timing of such a reduction is currently highly uncertain. Meanwhile, recent studies indicate that using climate models with high enough ocean resolutions to simulate mesoscale eddies improve simulated winter Euro-Atlantic blocking events significantly. In this paper, we show from a large ensemble of climate simulations based on the highest emission scenario that largely prominent and coarsely resolved non-eddying climate models project a noticeable significant decline in blocking frequencies from the 2030s-2040s, whereas blocking statistics in eddy-permitting simulations are noticeably decreasing only from years 2060s. Our result suggests with a strong level of confidence that winter blocking activity over the next several decades will keep being dominated by internal variability.

1. Introduction:

Atmospheric blocking is defined by large synoptic-scale pressure anomalies at midlatitudes that alter the midlatitude jet stream's pathways and redistribute precipitation and temperatures across many regions (Woolings et al. 2018). These pressure anomalies can last several days, thereby causing persistent weather extreme conditions at several locations (Kautz et al. 2022). The nature and amplitudes of underlying extremes depend on the timing of the blocking event (Davini and D'Andrea 2020), the location of blocked areas (Brunner et al. 2018), and background climate conditions (De Vries et al. 2013, Kautz et al. 2022, Woolings et al. 2018).

Winter blocking events occur frequently in the Euro-Atlantic sector and have a considerable impact on winter regimes across Europe (Cassou et al. 2004, Michel et al. 2023, Terray et al. 2005). These winter blocking conditions result in droughts (Sillman and Croci-Maspoli 2009), heavy precipitation (Kautz et al. 2022), extreme snowfalls (Cattiaux et al. 2011, de Vries et al. 2013), or cold spells (Cattiaux et al. 2010), all of which can have considerable impact on socioeconomic sectors such as energy or agriculture (Woolings et al. 2018).

Upper-level tropical warming and near-surface Arctic warming are expected to result in stronger zonal winds and consequently in fewer Winter Euro-Atlantic Blocking (WEAB) events (Kennedy et al. 2016, Woolings et al. 2018). A wide range of studies showed that most state-of-the-art General Circulation Models (GCMs) of climate of the last three phases of the Coupled Model Intercomparison Project (CMIP3, CMIP5 and CMIP6) simulate this decrease in WEAB frequencies far before the end of the century, both for moderate and large emission scenarios (Davini and D'Andrea 2020, Dunn-Singouin and Sun 2013, Fabiano et al. 2021, Kennedy et al. 2016, Masato et al. 2013, Matsueda and Endo 2017, Sillman and Croci-Maspoli 2009). However, Bacer et al. (2022) recently showed no significant decrease in WEAB frequencies for half of the simulations from six CMIP6 GCMs (selected for their relatively good performance in simulating

historical WEAB frequencies observations) by the end of the century and under the highest emission scenario (SSP5-8.5). Also, CMIP5 GCMs generally do not simulate significant changes in future structures of main winter Euro-Atlantic patterns (Huguenin et al. 2020). Woolings et al. (2018) already emphasized that the large disparity in projected WEAB frequencies from GCMs (Masato et al. 2013) and their generally poor ability to simulate observed WEAB events (Davini and D'Andrea 2016), both cause large uncertainties on the occurrence, and if so, the timing of a decline in WEAB frequencies under climate change.

The ability of GCMs to simulate WEAB is notably hampered by extensively documented persistent biases, such as in simulated tropical convection (Gollan et al. 2019), transient eddy forcing (Berckmans et al. 2013, Davini et al. 2017), model orography (Berckmans et al. 2013), or sea surface temperatures (Athanasiadis et al. 2022, Michel et al. 2023, Scaife et al. 2011). Increased atmospheric resolution was shown to improve the simulation of WEAB events notably through reduced biases in simulated transient eddies (Davini et al. 2017, 2021) and improved orographic resolution (Berckmans et al. 2013). Two recent studies illustrated that the bias reduction in simulated sea surface temperature patterns achieved from the presence of mesoscale eddy-permitting (EP) ocean models also improves the simulation of WEAB events from GCMs (Athanasiadis et al. 2022, Michel et al. 2023). These results were explained by reduced biases in sea surface temperature gradients (Athanasiadis et al. 2022) shaped by better representation of oceanic fronts (Hewitt et al. 2016, 2020, Michel et al. 2023, Scaife et al. 2011). This improves the realism of simulated low level baroclinicity and vertical heat and moisture fluxes contributing to blocking genesis (Cheung et al. 2023, O'Reilly et al, 2016). Earlier studies on future WEAB behavior were predominantly based on GCM simulation ensembles mostly composed of less accurate non-eddying (NE) GCMs, which are still highly prominent in CMIP6 (Eyring et al. 2016). Therefore, the present study seeks at refining projections of future WEAB activity in the context of climate change by comparing two extensive sets of EP and NE GCM future simulations.

2. Data and Methods:

2.1. Data:

We employ up to 58 future simulations from 21 GCMs that participated to CMIP6 and High resolution MIP (HighresMIP)/PRIMAVERA activities (Supplementary Table S1). We focus our investigation only on simulations for the largest greenhouse gas emission experiments (i.e., SSP5-8.5), as HighResMIP/PRIMAVERA future simulations were conducted only for this future scenario (Haarsma et al. 2016). Therefore, 17 future simulations were taken from the highres-future experiment of the HighResMIP/PRIMAVERA activity, and 41 were taken from the SSP5-8.5 experiment of the ScenarioMIP CMIP6 activity. We choose up to four simulation members per GCM/experiment pair where available to account for the influence of the large internal variability in simulated WEAB events (Supplementary Table S1).

It must be noted that EP GCMs are rare in CMIP6 future simulations but more common in HighResMIP/PRIMAVERA future simulations, where the majority ends in 2050. As a result, future GCM simulations will be studied for different periods: near future (NF, 2015-2050), far future (FF, 2051-2099), and the 21st century (21C,2015-2099), with 21C representing simulations from NF that have been conducted until at least 2099 (Supplementary Table S1). In the end, NF is made up of 16 EP simulations and 42 NE simulations (58 in total), while FF and 21C are made up of 7 EP simulations and 35 NE simulations (42 in total, Supplementary Table S1). It should be emphasized that only a single NF simulation (HadGEM3-GC31-HH) was produced by a GCM with an ocean resolution higher than 0.1°x0.1°, which is considered eddy-rich. However, because just one of these simulations is being investigated here, it will be handled in the EP GCM group in the section that follows.

Finally, we will compare the results of future simulations for NF and FF periods to those in present-day simulation outputs using 61 additional historical simulations from 1979 to 2014 based on fairly comparable GCM simulations ensembles (15 EP and 46 NE simulations, Supplementary Table S1). Ultimately, the present study is based on a very large ensemble of 119 simulations, both future (58) and historical (61) (Supplementary Table S1).

In the following, data from the different GCM simulations used (Supplementary Table S1) are initially interpolated on regularly separated 1°x1° grids.

2.2. Methods:

2.2.1 Blocking detection

We detect blocking events using on a long-established technique based on daily 500 hPa geopotential heights (Z500) fields providing a time-varying 2-dimensionnal blocking index (Sherrer et al. 2006). Other techniques, for instance based on potential vorticity fields or Z500 anomalies (Woolings et al. 2018) are more biased in the context of transient climate variations.

The method is based on detecting blocking situations for each grid point wherever a reversal in the meridional geopotential heights gradient is observed. Therefore, we consider that a given grid point with longitude λ_0 and latitude ϕ_0 is blocked at time t if the three following conditions $C1 - C3$ are fulfilled:

$$C1: GHGS(\lambda_0, \phi_0) > 0$$

$$C2: GHGN(\lambda_0, \phi_0) < -10$$

$$C3: GHGS_2(\lambda_0, \phi_0) < -5$$

$GHGS$, $GHGN$, and $GHGS_2$ are given by:

$$GHGS(\lambda_0, \phi_0) = \frac{Z500(\lambda_0, \phi_0) - Z500(\lambda_0, \phi_S)}{\phi_0 - \phi_S}$$

$$GHGN(\lambda_0, \phi_0) = \frac{Z500(\lambda_0, \phi_N) - Z500(\lambda_0, \phi_0)}{\phi_N - \phi_0}$$

$$GHGN(\lambda_0, \phi_0) = \frac{Z500(\lambda_0, \phi_S) - Z500(\lambda_0, \phi_{S_2})}{\phi_S - \phi_{S_2}}$$

With $\phi_S = \phi_0 - 15°$, $\phi_N = \phi_0 + 15°$, and $\phi_{S_2} = \phi_0 - 30°$. Therefore, for a given spatial field $\{\Lambda, \Phi\}$ and for n daily timesteps, the 2D blocking index defined as:

$$M(\lambda, \phi, t) = \begin{cases} 1 \; if \; C1 \; \cap \; C2 \cap C3 \\ 0 \; otherwise \end{cases}, \lambda \in \Lambda, \phi \in \Phi, \mathrm{t} = \mathrm{t}_1, \dots, \mathrm{t}_n$$

In addition, all grid points in $\{\Lambda, \Phi\}$ that are blocked for less than four days are turned to 0 to avoid spurious detection of short-term, not impactful, and isolated blocking conditions across the grid (Davini et al. 2012, Davini et al. 2017, Michel et al. 2023).

2.2.2 Blocking clustering

Clustering atmospheric blocking patterns is a common task that enables to study blocking activity in terms of both frequencies and spatial patterns in an automatic way and has been used frequently (Bacer et al. 2022, Cassou et al. 2004, Fabiano et al. 2021, Michelangeli et al. 1995, Michel et al. 2023, Terray et al. 2005). However, these studies differ with respect to the variable that is used for clustering blocking patterns, namely: sea level pressure (Cassou et al. 2004, Terray et al. 2005), geopotential heights at 700 hPa (Michelangeli et al. 1995), principal components of Z500 (Fabiano et al. 2021), and 2D blocking index of blocking conditions longer than 4 days (Michel et al. 2023). The clustering here consists of clustering days (winter ones here, *i.e.* days from December, January, and February) based on their pattern similarities. This approach is useful to study different types of blocking patterns and their respective frequencies, as they were shown to have different and sometimes opposite meteorological fingerprints (Michel et al. 2023). Using such an approach, for instance, Fabiano et al. (2021) evaluated, using a large ensemble of CMIP5 and CMIP6 GCM simulations, that only specific blocking patterns were significantly decreasing in the future as a result of rising temperatures. The clustering used here

(Michel et al. 2023) includes much less noisy signals than pressure variables (*i.e.* sea level pressure and geopotential heights) used by other studies (Cassou et al. 2004, Fabiano et al. 2021, Michelangeli et al. 1995, Terray et al. 2005). For the k-means to be applied such that days are clustered based on their blocking pattern similarities, the 3D matrix M is turned into a 2D matrix denoted X, where rows are time steps and columns are all the grid points in $\{\Lambda, \Phi\}$ (Michel et al. 2023). First, k centroids $\mu_1^{(1)}, \dots, \mu_k^{(1)}$ for respective clusters $c_1^{(1)}, \dots, c_k^{(1)}$ are first randomly drawn in the $\{\Lambda, \Phi\}$ space and blocking patterns for each time step are affiliated to the cluster with the closest centroid in terms of Euclidian distance. This procedure is repeated until convergence (when centroids stop changing), where the update of centroids at each occurrence is given by:

$$\mu_j^{(t+1)} = \frac{1}{\#\{c_j^{(t)}\}} \sum_{i \in c_j^{(t)}} X_i \, , j = 1, \dots, k$$

Each k-means model in the study is ran 200 times with different random initializations of centroids. The set of random initial centroids with lowest Euclidian distances between cluster members and their respective centroid is retained. The k parameter is generally chosen from reanalysis data using optimization methods (Cassou et al. 2005, Michel et al. 2023). However, former studies did not necessarily found or used similar values: k=4 (Cassou et al. 2005, Fabiano et al. 2020, 2021, Terray et al. 2005), k=5 (Michel et al. 2023) or k=6 (Falkena et al. 2020) WEAB types. Here, as we used the clustering based on the same variable as Michel et al. (2023), we use the parameter *k=5* and will refer to the five main patterns identified from ERA5 as: Western Europe (WE), Greenland (Gr.), North Sea (NS), Baltic Sea (BS) and Scandinavia (Sc.).

In ERA5 data, this clustering for 5 main WEAB pattern is made with a *k=6* parameter where only the above five clustered patterns are kept. The 6th cluster constitute a “neutral” or “non-blocking” group and accounts for about 72% of all DJF days in ERA5 between 1979 and 2014 (Michel et

al. 2023). For GCMs, we attribute each daily blocking pattern to the closest centroid based on Euclidian distances. In this procedure, the “neutral” group from the reanalysis clustering is also used to allow the attribution of GCM blocking patterns to this category when they are not resembling one of the other five.

3. Results:

Spatial distribution of projected WEAB frequencies and trends

Mean projected blocking frequencies averaged throughout the NF period (2015-2050) for both NE and EP GCM ensembles (Supplementary Table S1) are shown in Fig. 1a,b, and significant differences at the 90% confidence level between the ensembles are shown in Fig. 1c. It appears that EP GCMs simulate a significantly higher number of blocking events by 2050, where significant differences cover most regions of high blocking occurrence identified by previous studies, such as Greenland, Nordic Sea, or Scandinavia (Fig. 1a-c, Fabiano et al. 2021, Michel et al. 2023, Terray et al. 2005). Furthermore, we see a wide area including the Baltic and Nordic seas, British Islands, and the northeastern Atlantic where blocking frequency trends are notably negative in the NE GCM ensemble (Fig. 1d). For EP GCMs, on the other hand, two tiny areas with positive (Iceland) and negative (Greenland) trends are detected, but the fraction of grid points with significant trends is lower than the 10% first species risk of the Student t-test used (7%, Fig. 1e). According to this preliminary analysis EP GCMs simulate more blocking events on average by 2050 than NE GCMs (Fig. 1a-c) and also do not project any significant decrease in frequencies until 2050 (Fig. 1d,e).

The increased simulated blocking frequencies found for EP GCMs over the historical (Michel et al. 2023) and NF periods (Fig. 1a-c) persist during the *21C* period (Fig. 1f-h). However, the geographical range of significant differences between the two groups is smaller than what we found for NF (Fig. 1c,h). In terms of trends, both model groups show significantly lower blocking

frequencies throughout the *21C* period. These significant decreases are geographically consistent in the NE GCM simulation ensemble, but not in the EP ones, although most locations with high blocking prominence experience a significant decline (Fig. 1i-j). Supplementary Fig. S1 shows the same ensemble analyses as Fig. 1 for the historical simulations from Supplementary Table S1, where EP GCM WEAB frequencies are higher, consistent with Athanasiadis et al. 2022 and Michel et al. 2023, and also show significant decrease in NE simulations but not in EP simulations.

To further test the robustness of the above findings across GCMs, Monte Carlo tests and Student t-tests based on area-averaged blocking frequencies and trends were performed over the study area (50W-50E, 30-72.5N) for three GCM simulation periods: historical (1979-2014, hist), NF, and *21C* (Supplementary Table S1, Fig. 2). For the three periods, the Monte-Carlo tests determine confidence levels based on proportions of mean blocking frequencies from NE GCM samples of same size as the smaller EP GCM ensembles (Fig. 2a). For hist and NF, it appears that none of the 10,000 randomly drawn NE simulation samples have mean area-averaged blocking frequencies that reach the one of the EP GCM simulations (Fig. 2a), which strongly supports the results shown in Fig. 1. The significance level for *21C*, on the other hand, is lower but still higher than 95% (Fig. 2a), also consistent with differences seen between Fig. 1c and Fig. 1h.

For trends, Student t-tests show that both 95% and 99% confidence intervals for mean area-averaged trends from NE GCM simulations do not include 0 for all three periods, including hist (Fig. 2b). On the other hand, EP GCM simulations only indicate significantly decreasing blocking frequencies at the 99% confidence level when the entire 21st century is taken into account, but trends are not significant for NF and hist. This result demonstrates that the response in WEAB frequencies to strong anthropogenic forcing differs significantly between EP and NE simulations, with EP GCMs simulating the same lower blocking frequencies far later in the century than NE GCMs. Furthermore, as observed in historical simulations (Athanasiadis et al. 2022, Michel et al.

2023, Supplementary Fig. S1), EP GCMs simulate substantially higher and likely more realistic WEAB frequencies for both NF and 21C periods (as they do so for historical, Michel et al. 2023), implying that such GCMs are better suited to studying future winter blocking in Europe.

Future evolution of observed main WEAB patterns

In addition to the spatial analyses shown in Figs. 1-2, we clustered WEAB events in both historical and future simulations into five primary blocking patterns, as performed in previous studies (Cassou et al. 2004, Fabiano et al. 2021, Falkena et al. 2020, Michelangeli et al. 1994, Michel et al. 2023, Terray et al. 2005).

We find no significant changes in the mean spatial extent of simulated blocking patterns over time, and neither EP nor NE GCM demonstrate any significant shift in the location of their assigned patterns (Fig. 3a,d,g,j,m). Indeed, for each blocking footprint, the simulated WEAB frequency tends to be more sensitive to NE and EP ocean configurations than to increasing temperatures, although the configuration effect is relatively small.

In terms of temporal evolution of these blocking patterns, we observe that the WEAB response to anthropogenic forcing differs significantly over time, both between the NE and EP GCM ensembles and between the simulated blocking patterns (Fig. 3b,e,h,k,n). Based on trends evaluated across 36-year intervals (i.e., the same size as hist and NF periods), we find that frequencies from a particular blocking type (i.e., Baltic Sea) do not show a globally consistent decline over time for both NE and EP GCM ensembles (Fig. 3k,l). Greenland blocking declines considerably more consistently in NE GCMs than in EP GCMs, where just a few 36-year slices show significant decreases, although these are sufficient to significantly reduce Greenland blocking occurrence by the end of the century (Fig. 3e,f). The opposite is true for Scandinavian

blocking, which has a significant decrease in frequency in EP GCM simulations late in the century (from about 2060), but no globally significant decline in NE GCM simulations (Fig. 3n,o). Both NE and EP GCM ensembles suggest a decline in frequencies after 2050 for the most prevalent Western Europe blocking events (Michel et al. 2023), however the trend appears to be mitigated at decadal to multidecadal time frames for EP GCMs (Fig. 3b,c). Furthermore, EP GCMs show a time frame between 2000 and 2040 where Western Europe's blocking frequencies increase significantly. Finally, WEAB frequencies over the Nordic Sea drop in both GCM groups, but the timing differs considerably, occurring between 2015-2060 for NE GCMs and 2030-2085 for EP GCMs.

Global view of future WEAB activity

Substantial disparities in simulated future WEAB frequencies exist between the NE and EP GCMs, both geographically (Figures 1 and 2) and temporally (Figure 3). In Fig. 4, we present an overall summary of results depicted above, where we show the total WEAB frequencies for EP and NE ensembles (Fig. 4a) estimated as the sums of ensemble-means of timeseries from each simulated blocking pattern for NE and EP GCMs, (Fig. 4b), as well as successive 36-year trends of these timeseries. The magnitude of trends presented in Fig. 4b cannot be directly compared between EP and NE simulation ensembles because they were computed from time series with significantly different averages (Michel et al. 2023).

The assumption that EP GCMs have a smaller WEAB response to anthropogenic forcing than NE GCMs derived from spatially distributed trends (Figs. 1-2) and several of the clustered blocking patterns (Fig. 3) is confirmed here for the total frequencies for all blocking patterns (Fig. 4). Indeed, we find that total WEAB frequencies in NE GCMs start decreasing significantly (at the 95% confidence level) for 36-year time frames as early as 2000 (thus centered around 2018 and noticed around 2036) and continue to decrease significantly for following time frames until the

end of the century (Fig. 4). The ensemble of EP GCM simulations tells a completely different story, as 36-year trends in total WEAB frequencies start to be significantly and consistently negative only for time frames centered around 2040 (thus noticed around 2060), representing a more than 20-year delay compared to NE GCMS.

Beyond the significant downward trend in EP GCM WEAB frequencies found in the second half of the 21st century (Fig. 4), the ensemble mean of these GCMs shows alternate decadal to multidecadal periods with either significant or non-significant downward trends. This overall results in an overall decrease in WEAB frequencies for EP GCMs but contrasts sharply with the uninterruptedly significant negative trends observed over the entire 21st century for the NE GCM ensemble. Hence, EP GCMs appear to be responding less to human-caused rising temperatures (Fig. 1-4), and the role of decadal to multidecadal underlying processes such as those associated with the North Atlantic/Arctic Oscillation are more important in shaping future WEAB activity.

Conclusions and Discussion:

Our study was motivated by recent findings demonstrating higher accuracy in simulating WEAB frequencies for EP GCMs compared to much more prevalent NE GCMs in the current CMIP6 generation (Athanasiadis et al. 2022, Michel et al. 2023), whereas EP GCMs were simply absent in CMIP3 and CMIP5. Our results support those of most prior studies suggesting that the occurrence of WEAB events will be significantly reduced by the end of the century (Davini and D'Andrea 2020, Dunn-Singouin and Sun 2013, Fabiano et al. 2021, Kennedy et al. 2016, Masato et al. 2013, Matsueda and Endo 2017, Sillman and Croci-Maspoli 2009). However, we discovered significant differences in how NE and EP GCMs simulate the evolution of future WEAB events under high human-induced forcing (Figs. 1-4). Indeed, while NE GCMs suggest that WEAB frequencies may begin to decrease considerably over the next decade (Figs. 1, 4a), EP GCMs

suggest a delay of more than 20 years. These findings indicate that no significant decrease in the occurrence of blocking-related winter extremes in Europe is expected in the coming decades. Furthermore, we determined that EP GCMs simulate much more WEAB events in future simulations than NE GCMs as was found for historical simulations (Michel et al. 2023). Given the current need for a more precise picture on the future WEAB projections due to widely disparate projections from NE GCMs (Fig. 2, Woolings et al. 2018), the use of EP GCM simulations in future research is crucial.

In addition to the delayed response in decreased WEAB frequencies for EP GCMs, we also found that some 36-year long periods late in the century still experience no significant decrease (Fig. 4) whereas this is almost permanent in NE GCM simulations as early as from the 2030s. This result indicates a stronger role for internal variability in future WEAB occurrences in EP GCMs.

Due to the current low number of EP GCM simulations available in CMIP6 and HighResMIP/PRIMAVERA ensembles, we were unable to investigate other future simulations such as those under intermediate (e.g., SSP2-4.5 and SSP3-7.0) or low (e.g., SSP1-2.6) greenhouse gas emission scenarios. In this respect, Hausfather and Peters (2020) recalled that the most widely used and widely communicated future scenario (i.e. SSP5-8.5) that we study here is extremely useful for scientists attempting to understand the climate response to strong CO_2 forcings. However, its forcing is so large that it remains largely unlikely and unrealistic to effectively happen in reality given current socioeconomic trends (Hausfather and Peters 2020). As a result, the delayed decrease in WEAB frequencies found for EP GCMs over NE GCMs may be even larger in the real-world, because future CO_2 emissions may be lower than those prescribed for the GCM simulations investigated here (Hausfather and Peters 2020). Therefore, it is likely that no significantly decreasing WEAB frequencies are expected to be noticed over the next several decades, and internal variability may continue to primarily influence WEAB activity

throughout this time (Woolings et al. 2018). However, a thorough examination of the response of WEAB frequencies under more realistic emission scenarios in a large enough EP GCM simulation ensemble has yet to be performed to corroborate the aforementioned statement. Current CMIP6 simulations do not yet allow for such an important analysis, and modeling centers handling EP GCMs are encouraged to include simulations for intermediate emission scenarios in future CMIP updates.

If we had limited our research to the NF simulation period (2015-2050), for which most EP GCM simulations were done (Supplementary Table S1), we would have reached somewhat similar findings as we do now, but with a much more incomplete picture. Indeed, downward trends in WEAB frequencies in EP GCM simulations begin later than 2050, which would not have been noticed if restricting the analysis to NF. This also reinforces the necessity for longer future simulations using EP GCMs in future CMIP protocols, as these GCMs have been demonstrated to simulate several climate processes far more correctly thans the currently widely used NE GCMs (Athanasiadis et al. 2022, Delworth et al. 2012, Hewitt et al. 2016, 2020, Michel et al. 2023, Moreno-Chamarro et al. 2021, Roberts et al. 2018).

Open Research section

Data availability statement:

Original CMIP6 (Eyring et al. 2016) and HighResMIP/PRIMAVERA (Haarsma et al. 2016) data are available through CEDA Earth System Grid Federation portals (https://esgf-index1.ceda.ac.uk/search/cmip6-ceda/, https://esgf-index1.ceda.ac.uk/search/primavera-ceda/). ERA5 reanalysis data (Hersbach et al. 2020) are available on the Copernicus Climate Change Service (C3S) Climate Data Store (https://cds.climate.copernicus.eu/cdsapp#!/home). Data produced through the study are available on a Zenodo repository with following DOI: 10.5281/zenodo.8090836.

References:

- Athanasiadis, P. J., F. Ogawa N.-E. Omrani N. Keenlyside, R. Schiemann, A. J. Baker, P. J. Vidale, A. Bellucci, P. Ruggieri, R. Haarsma, M. Roberts, C. Roberts, L. Novak, and S. Gualdi (2022), Mitigating climate biases in the midlatitude North Atlantic by increasing model resolution: SST gradients and their relation to blocking and the jet, *Journal of Climate*, **35(21)**, 6985-7006, doi: 10.1175/JCLI-D-21-0515.1.

- Bacer S., F. Jomaa, J. Beaumet, H. Gallée, E. Le Bouëdec, M. Ménégoz, and C. Staquet (2022), Impact of climate change on wintertime European atmospheric blocking, *Weather and Climate Dynamics*, **3(1)**, 377-389, doi: 10.5194/wcd-3-377-2022.

- Berckmans, J., T. Woollings, M.-E. Demory, P.-J. Vidale, and M. Roberts. Atmospheric blocking in a high resolution climate model: influences of mean state, orography and eddy forcing, *Atmospheric Research Letters*, **14(1)**, doi: 10.1002/asl2.412.

- Brunner, L., N. Schaller, J. Anstey, J. Sillmann, and A. K. Steiner (2018), Dependence of Present and Future European Temperature Extremes on the Location of Atmospheric Blocking, *Geophysical Research Letters*, **45(12)**, 6311-6320, doi: 10.1029/2018GL077837.

- Cassou, C., L. Terray, J. W. Hurrell, and C. Deser (2004), North Atlantic winter climate regimes: Spatial asymmetry, stationarity with time, and oceanic forcing, *Journal of Climate*, **17(5)**, 1055-1068, doi: 10.1175/1520-0442(2004)017<1055:NAWCRS>2.0.CO;2.

- Cattiaux, J., R. Vautard, C. Cassou, P. Yiou, V. Masson-Delmotte, and F. Codron (2010), Winter 2010 in Europe: a cold extreme in a warming world, *Geophysical Research Letters*, **37(20)**, L20704, doi: 10.1029/2010GL044613

- Cheung, H.-N., N.-E.Omrani, F. Ogawa, N. Keenlyside, H. Nakamura, and W. Zhou (2023) Pacific oceanic front amplifies the impact of Atlantic oceanic front on North Atlantic blocking, *npj Climate and Atmospheric Science*, **6**, 61, doi: 10.1038/s41612-023-00370-x

- Davini, P., C. Cagnazzo, S. Gualdi, and A. Navarra (2012), Bidimensional diagnostics, variability, and trends of northern hemisphere blocking, *Journal of Climate*. **25**, 6496-6509, doi: https://doi.org/10.1175/JCLI-D-12-00032.1.

- Davini, P., S. Corti, F. D'Andrea, G. Rivière, and J. von Hardenberg (2017) Improved winter European atmospheric blocking frequencies in high-resolution global climate simulations, *Journal of Advances in Modeling Earth Systems*, **9**, 2615-2634, doi: 10.1002/2017MS001082.

- Davini, P., and F. D'Andrea (2020), From CMIP3 to CMIP6: Northern hemisphere atmospheric blocking simulation in present and future climate, *Journal of Climate*, **33(23)**, 10021-10038, doi: 10.1175/JCLI-D-19-0862.1.

- Davini, P., and F. D'Andrea (2016), Northern Hemisphere Atmospheric Blocking Representation in Global Climate Models: Twenty Years of Improvements?, *Journal of Climate*, **29(24)**, 8823-8840, doi: 10.1175/JCLI-D-16-0242.1

- Davini, P., A. Weisheimer, M. Balmaseda, S. J. Johnson, F. Molteni., C. D. Roberts, R. Senan, and T. N. Stockdale (2021), The representation of winter Northern Hemisphere atmospheric blocking in ECMWF seasonal prediction systems, *Quaternary journal of the Royal Meteorological Society*, **147(735)**, 1344-1363, doi: 10.1002/qj.3974.

- De Vries, H., T. Woolings, J. Antsey, R. J. Haarsma, and W. Hazeleger (2013), Atmospheric blocking and its relation to jet changes in a future climate change, *Climate Dynamics*, **41**, 2643-2654, doi: 10.1007/s00382-013-1699-7.

- Delworth, T. L., A. Rosati, W. Anderson, A. J. Adcroft, V. Balaji, R. Benson, K. Dixon, S. M. Griffies, H.-C. Lee, R. C. Pacanowski, G. A. Vecchi, Wittenberg, A. T., Zeng, F., and Zhang, R. (2012), Simulated Climate and Climate Change in the GFDL CM2.5 High-Resolution Coupled Climate Model, *Journal of Climate*, **25(8)**, 2755-2781, 10.1175/JCLI-D-11-00316.1.

- Dunn-Singouin, E., and S.-W. Son (2013), Northern Hemisphere blocking frequency and duration in the CMIP5 models, *JGR Atmospheres*, **118(3)**, 1179-1188, doi: 10.1002/jgrd.50143.

- Eyring, V., S. Bony, G. A. Meehl, C. A. Senior, B. Stevens, R. J. Stouffer, and K. E. Taylor (2016), Overview of the Coupled Model Intercomparison Project Phase 6 (CMIP6) experimental design and organization, *Geophysical Research Development*, **9(5)**,1937-1958, doi: 10.5194/gmd-9-1937-2016

- Fabiano, F, H. M. Christensen, K. Strommen, P. Athanasiadis, A. Baker, R. Schiemann, and S. Corti (2020), Euro-Atlantic weather Regimes in the PRIMAVERA coupled climate

simulations: impact of resolution and mean state biases on model performance *Climate Dynamics*, **54**, 5031-5048, doi: 10.1007/s00382-020-05271-w

- Fabiano, F., V. L. Meccia, P. Davini, P. Ghinassi, and S. Corti (2021), A regime view of future atmospheric circulation changes in northern mid-latitudes, *Weather and Climate Dynamics*, **2(1)**, 163-180, doi: 10.5194/wcd-2-163-2021.

- Falkena, S. K. J., J. de Wiljes, A. Weisheimer, T. G. Shepherd (2020), Revisiting the identification of wintertime atmospheric circulation regimes in the Euro-Atlantic sector, *Quarternary Journal of the Royal Meteorological Society*, 146(731), 2801-2814, doi: 10.1002/qj.3818.

- Gollan, G., S. Bastin, and R. J. Greatbatch (2019), Tropical precipitation influencing boreal winter midlatitude blocking, *Atmospheric Research* Letters, **20(5)**, doi: 10.1002/asl.900.

- Haarsma, R. J., M. J. Roberts, P. L. Vidale, C. A. Senior, A. Bellucci, Q. Bao, P. Chang, S. Corti, N. S. Fučkar, V. Guemas, J. von Hardenberg, W. Hazeleger, C. Kodama, T. Koenigk, L. R. Leung, J. Lu, J.-J. Luo, J. Mao, M. S. Mizielinski, R. Mizuta, P. Nobre, M. Satoh, E. Scoccimarro, T. Semmler, J. Small, and J.-S. von Storch (2016), High Resolution Model Intercomparison Project (HighResMIP v1.0) for CMIP6, *Geoscientific Model Development*, **9(11)**, doi: 10.5194/gmd-9-4185-2016

- Hausfather, Z., and G. P. Peters (2020), Emissions – the 'business as usual' story is misleading, *Nature*, **577**, 618-620, doi: 10.1038/d41586-020-00177-3

- Hersbach, H., B. Bell, P. Berrisford, S. Hirahara, A. Horányi, J. Muñoz-Sabater, J. Nicolas, C. Peubey, R. Radu, D. Schepers, A. Simmons, C. Soci, S. Abdalla, X. Abellan, G. Balsamo, P. Bechtold, G. Biavati, J. Bidlot, M. Bonavita, G. De Chiara, P. Dahlgren, D. Dee, M. Diamantakis, R. Dragani, J. Flemming, R. Forbes, M. Fuentes, A. Geer, L. Haimberger, S. Healy, R. J. Hogan, E. Hólm, M. Janisková, S. Keeley, P. Laloyaux, P. Lopez, C. Lupu, G. Radnoti, P. de Rosnay, I. Rozum, F. Vamborg, D. Villaume, and J.-N. Thépaut (2020), The ERA5 global reanalysis, *Quaternary Journal of the Royal Meteorological Society*, **146(730)**, 10.1002/qj.3803.

- Hewitt, H. T., M. J. Roberts, P. Hyder, T. Graham, J. Rae, S. E. Belcher, R. Bourdallé-Badie, D. Copsey, A. Coward, C. Guiavarch, C. Harris, R. Hill, J. J.-M. Hirschi, G. Madec, M. S. Mizielinski, E. Neininger, A. L. New, J.-C. Rioual, B. Sinha, D. Storkey, A. Shelly, L. Thorpe, and R. A. Wood (2016), The impact of resolving the Rossby radius at mid-latitudes in the ocean: results from a high-resolution version of the Met Office GC2 coupled model, *Geoscientific Model Development*, **9(10)**, doi: 1 **0.5194/gmd-9-3655-2016.**

- Hewitt, H. T., M. Roberts, P. Mathiot, A. Biastoch, E. Blockley, E. P. Chassignet, B. Fox-Kemper, P. Hyder, D. P. Marshall, E. Popova, A.-M. Treguier, L. Zanna, A. Yool, Y. Yu, R. Beadling, M. Bell, T. Kuhlbrodt, T. Arsouze, A. Bellucci, F. Castruccio, B. Gan, D. Putrasahan, C. D. Roberts, L. Van Roekel, and Q. Zhang (2020), Resolving and parameterising the ocean mesoscale in Earth system models, *Current Climate Change Reports*, **6**, 137-152, doi: 10.1007/s40641-020-00164-w.

- Huguenin, M. F., E. M. Fischer, S. Kotlarski, S. C. Scherrer, C. Schwierz, R. Knutti (2020) Lack of Change in the Projected Frequency and Persistence of Atmospheric Circulation

481 Types Over Central Europe, *Geophysical Research Letters*, **47(9)**, doi:
482 10.1029/2019GL086132.
483
484 - Kautz, L.-A., O. Martius, S. Pfahl, J. G. Pinto, A. M. Ramos, P. M. Sousa, and Tim
485 Woolings (2022), Atmospheric blocking and weather extremes over the Euro-Atlantic
486 sector – a review, *Weather and Climate Dynamice*, **3(1)**,305-336, doi: 10.5194/wcd-3-305-
487 2022.
488
489 Kennedy, D., T. Parker, T. Woollings, B. Harvey, L. Shaffrey (2016), The response of high-
490 impact blocking weather systems to climate change. *Geophysical Rsearch Letters*.
491
492 - Masato, G., B. J. Hoskins, and T. Woolings (2013), Winter and Summer northern
493 hemisphere blocking in CMIP5 models, *Journal of Climate*, **26(18)**, 7044-7059, doi:
494 10.1175/JCLI-D-12-00466.1.
495
496 - Matsueda, M., and H. Endo (2017), The robustness of future changes in Northern
497 Hemisphere blocking: A large ensemble projection with multiple sea surface temperature
498 patterns, **44(10)**, 5158-5166, doi: 10.1002/2017GL073336
499
500 - Michelangeli, P.-A., R. Vautard, and B. Legras (1995), Weather regimes: recurrence and
501 quasi stationarity, *Journal of the Atmospheric Sciences*, **52(8)**, 10.1175/1520-
502 0469(1995)052<1237:WRRAQS>2.0.CO;2.
503
504 - Michel, S. L. L., A. S. von der Heydt, R. M. van Westen, M. L. J. Baatsen, and H. A. Dijkstra
505 (2023), Increased wintertime European atmospheric blocking frequencies in general

506 circulation models with an eddy-permitting ocean, *npj Climate and Atmospheric Science*,
507 **6**, 50, doi: 10.1038/s41612-023-00372-9
508
509 - Moreno-Chamarro, E., L.-P. Caron, P. Ortega, S. Loosveldt Tomas, and M. J. Roberts
510 (2021), Can we trust CMIP5/6 future projections of European winter precipitation?
511 *Environmental Research Letters*, **16(5)**, doi: 10.1088/1748-9326/abf28a.
512
513 - O'Reilly, C. H., S. Minobe, and A. Kuwano-Yoshida (2015), The influence of the Gulf
514 Stream on wintertime European blocking, *Climate Dynamic*, **47**, 1545-1567, doi:
515 10.1007/s00382-015-2919-0
516
517
518 - Pfister, C., R. Weingartner, and J. Luterbacher, Hydrological winter droughts over the last
519 450 years in the Upper Rhine basin: a methodological approach, *Hydrological Sciences*
520 *Journal*, **51(5)**, 966-985, doi: 10.1623/hysj.51.5.966
521
522 - Roberts, M. J., P. L. Vidale, C. Senior, H. T. Hewitt, C. Bates, S. Berthou, P. Chang, H. M.
523 Christensen, S. Danilov, M.-E. Demory, S. M. Griffies, R. Haarsma, T. Jung, G. Martin, S.
524 Minobe, T. Ringler, M. Satoh, R. Schiemann, E. Scoccimarro, G. Stephens, and M. F.
525 Wehner (2018), The benefits of global high resolution for climate simulation: process
526 understanding and the enabling of stakeholder decisions at the regional scale, *Bulletin of*
527 *the American Meteorological Society*, **99(11)**, 2341-2359, doi: 10.1175/BAMS-D-15-
528 00320.
529
530 - Scherrer, S. C., M. Croci-Maspoli, C. Schwierz, C. Appenzeller (2006), Two-dimensional
531 indices of atmospheric blocking and their statistical relationship with winter climate

patterns in the Euro-Atlantic region, *International Journal of Climatoloy*, **26(2)**, 233-249, doi: 10.1002/joc.1250.

- Sillman, J., and M. Croci-Maspoli (2009), Present and future atmospheric blocking and its impact on European mean and extreme climate, **36(10)**, L10702, doi: 10.1029/2009GL038259

- Terray, L., M.-E. Demory, M. Déqué, G. de. Coetlognon, and E. Maisonnave. Simulation of late twenty-first century changes in wintertime atmospheric circulation over Europe due to anthropogenic causes (2005), *Journal of Climate*, **17(24)**, 4630-4635, doi: 10.1175/JCLI-3244.1.

- Woolings, T., D. Barriopedro, J. Methven, S.-W Son, O. Martius, B. Harvey, J. Sillman, A. R. Lupo, and S. Seneviratne (2018), Blocking and its response to climate change, *Current Climate Change Reports*, **4**, 287-300, doi: 10.1007/s40641-018-0108-z.

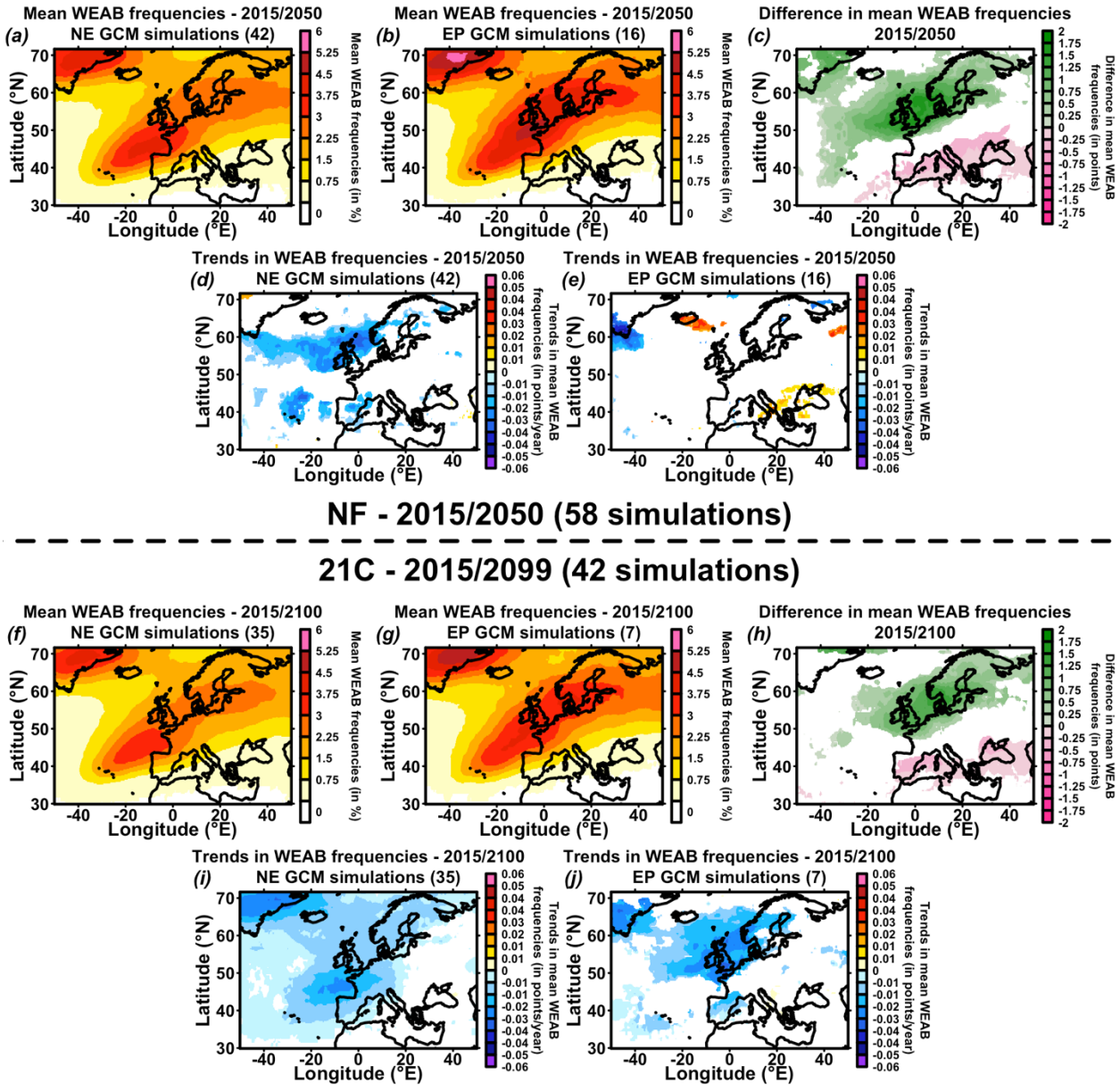

Figure 1: (a,b) Mean Winter Euro-Atlantic Blocking (WEAB) frequencies averaged over the near future (NF) period (2015-2050) in 42 non-eddying (NE) and 16 eddy-permitting (EP) General Circulation Model (GCM) future simulations under the highest greenhouse gas emissions scenario. (c) Difference in mean WEAB frequencies between EP (b) and NE (a) GCM simulations. Green colors indicates where WEAB frequencies are significantly higher in EP (resp. NE) GCM simulations at the 90% confidence level based on a two-tailed Student t-test. White colors indicate where there is no significant difference in WEAB frequencies from NE and EP GCMs based on the same test.

(d,e) Trends in percentage points per year in WEAB over the period under the highest greenhouse gas emission scenario, for NE and EP GCMs respectively. White colors indicate where trends are not significant at the 90% confidence level based on two-tailed regression slop Student t test. (f-j) Same as (a-e) for the 21C period (2015-2099) in 35 NE and 7 EP GCM simulations.

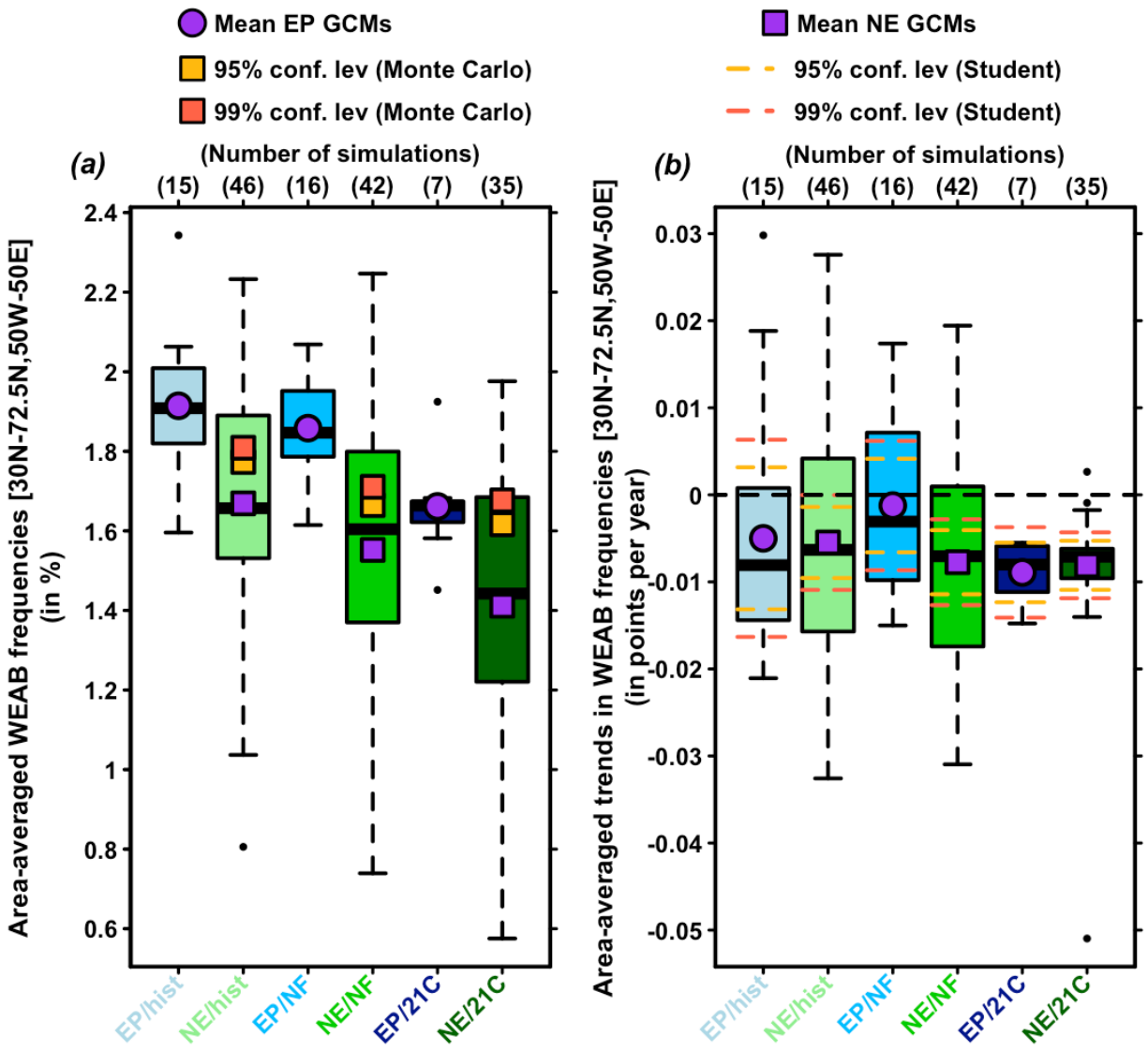

Figure 2: Area-averaged WEAB frequencies (a) and trends (b) over the study area: 50W-50E, 30N-72.5N. Light, normal, and dark blue (resp. green) boxplots give WEAB frequencies EP (resp. NE) GCM simulations for hist (1979-2014), NF (2015-2050) and 21C (2015-2100). Purple circles (resp. squares) indicate averages for each boxplot EP (resp. NE) GCM simulations group. (a) Yellow and red squares indicate 95% and 99% Monte-Carlo significance levels for EP GCM area averages. These levels are determined for each period (hist, NF, 21C) by sampling 10,000 groups of NE GCMs with the same number of GCM ensembles. (b) Yellow and red dashed lines indicate 95% and 99% Student confidence interval for each boxplot. The horizontal black dashed line indicates the 0 value.

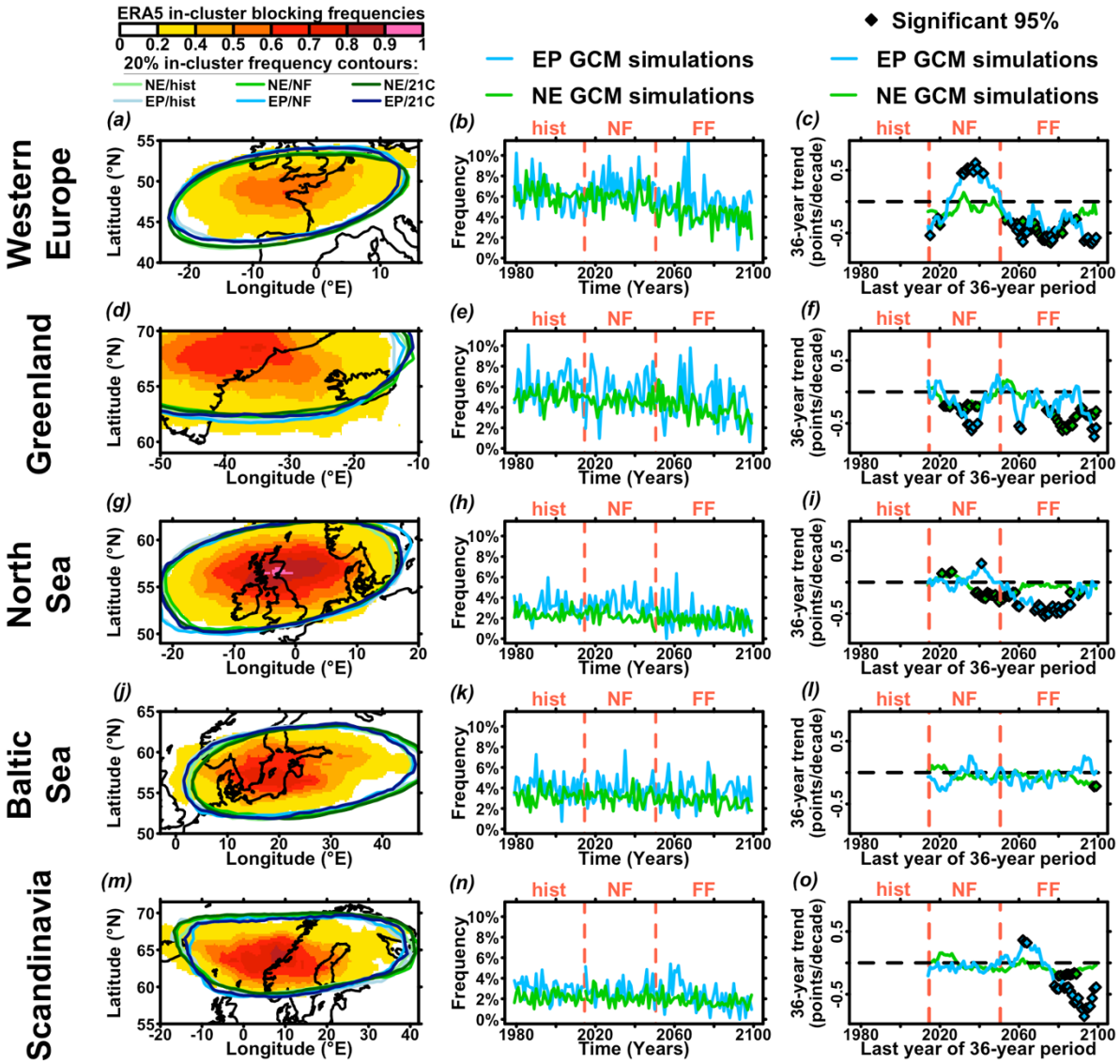

Figure 3: (a) ERA5 in-cluster blocking frequencies (colors) together with 20% contours of EP (resp. NE) GCM ensembles given as light, normal, and dark green (resp. blue) lines for hist (1979-2014), NF (2015-2050) and FF (2051-2100) periods, respectively. For the Western Europe blocking type. (b) Blue (resp. green) line indicates the composite time series of blocking frequency available EP (NE) GCM simulations over hist, NF, and FF periods. Vertical red lines separate hist, NF, and FF periods. For the Western Europe blocking type. (c) Trends in blocking frequencies over 36-year time frames calculated as linear regression slopes of blocking frequencies against time. Diamonds indicate regressions slopes significant at the 95% confidence level based on a

Student t-test. Results for EP (resp. NE) GCM ensembles are indicated with blue (resp. green) colors. Vertical red lines separate hist, NF, and FF periods. The horizontal black dashed line indicates the 0 value. For the Western Europe blocking type. (d-f) Same as (a-c) for the Greenland blocking type. (g-i) Same as (a-c) for the North Sea blocking type. (j-l) Same as (a-c) for the Baltic Sea blocking type. (m-o) Same as (a-c) for the Scandinavia blocking type.

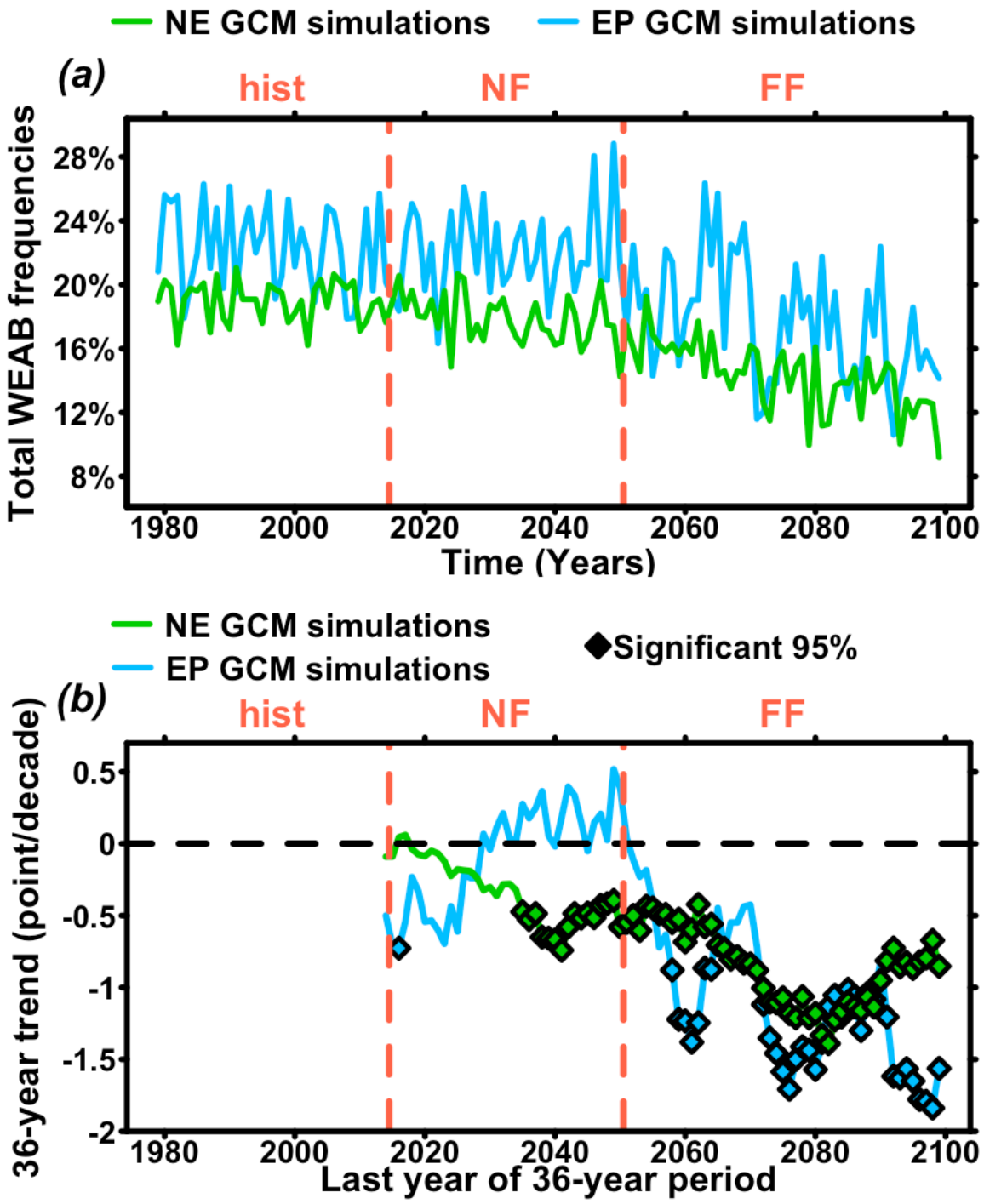

591

592 *Figure 4: (a) Composite time series of total frequencies of clustered blocking patterns for EP (blue)*

593 *and NE (GCMs). Vertical red lines separate hist, NF, and FF. (b) Trends in composite total*

594 *blocking frequencies over 36-year time frames calculated as linear regression slopes of blocking*

frequencies against time for EP (blue) and NE (green) GCM simulations. Diamonds indicate regressions slopes significant at the 95% confidence level based on a Student t-test. Vertical red lines separate hist, NF, and FF periods. The horizontal black dashed line indicates the 0 value.